Surfaces and Interfaces 38 (2023) 102792

Contents lists available at ScienceDirect

Surfaces and Interfaces

journal homepage: www.sciencedirect.com/journal/surfaces-and-interfaces

Concurrent study of the electrochemical response and the surface alterations of silver nanowire modified electrodes by means of EC-AFM. The role of electrode/nanomaterial interaction

Jose Luis Pura [a,b,*], Coral Salvo-Comino [a,b], Cristina García-Cabezón [b,c], María Luz Rodríguez-Méndez [a,b]

[a] Group UVASENS, Escuela de Ingenierías Industriales, Universidad de Valladolid, Paseo del Cauce, 59, Valladolid 47011, Spain
[b] BioecoUVA Research Institute, Universidad de Valladolid, Valladolid 47011, Spain
[c] Department of Materials Science, Universidad de Valladolid, Paseo del Cauce, 59, Valladolid 47011, Spain

ARTICLE INFO

Keywords:
EC-AFM
Cyclic voltammetry
Langmuir-blodgett
Silver nanowires
Electrochemical impedance spectroscopy

ABSTRACT

The use of nanomaterials as electrode modifiers permits the enhancement of electrode performance using a great variety of approaches, from electrocatalytic enhancement to the improvement of charge transfer processes. The control and understanding of the interaction between the modifiers and the electrode itself are of key importance for the final performance of the modified electrode. This becomes especially relevant in the case of nanostructured materials since their physical response is rarely trivial.

In this work, we combined electrochemistry and atomic force microscopy (EC-AFM) to in-situ investigate the surface condition of electrodes modified with silver nanowires (AgNWs) during EC measurements for the first time. EC-AFM allows us to perform cyclic voltammetry and electrochemical impedance spectroscopy together with the assessment of the electrode surface directly in the electrolytic solution. On the other hand, the use of the Langmuir-Blodgett technique provides homogeneity and reproducibility to the electrode modification process.

The electrochemical response of the modified electrodes has been found to strongly depend on the selected substrate, but also on the deposition procedure. This opens the path for a better understanding of electrode modification process, and also supports the viability of EC-AFM on open problems involving electrochemistry and surface science.

1. Introduction

There is a permanent search for new materials to be used as electrodes in electrochemical experiments. A great variety of ideas have been proposed for both the electrodes themselves [1–3] and also for potential candidates for electrode surface modification [4–7]. Nanomaterials are known to particularly excel in this last group. Firstly, because their reduced dimension boosts their surface/volume ratio, this immediately translates into better electrochemical activity as compared to their bulk counterparts [8]. On the other hand, nanomaterials also present unique properties as a result of their low dimensionality, making them excellent electrocatalytic materials. For instance, Ag nanowires (AgNWs) show exceptional electrical conductivity and are able to substantially improve charge transfer between the analyte and the electrode [9,10]. Furthermore, the AgNWs synthesis process is relatively simple and the use of silver provides a highly reduced fabrication cost as compared with other noble metals like Au or Pt. Regarding the development of the investigation surrounding these nanomaterials, their outstanding electrochemical properties tend to place the research focus on their response as improved sensors [11–15] or the electrode corrosion process [16,17]. However, relatively little work has been dedicated to a thorough characterization of the surface state [18] and the electrode/modifier interaction.

Among all the deposition techniques for thin, ordered,

Abbreviations: AA, Arachidic Acid; AgNW, Ag Nanowires; BDD, Boron-Doped Diamond; CV, Cyclic Voltammetry; EC, Electrochemistry; EC-AFM, Electrochemistry Atomic Force Microscopy; EDX, Energy Dispersive X-ray Spectroscopy; EIS, Electrochemical Impedance Spectroscopy; ITO, Indium Tin Oxide; LB, Langmuir-Blodgett; SEM, Scanning Electron Microscopy.

* Corresponding author at: Group UVASENS, Escuela de Ingenierías Industriales, Universidad de Valladolid, Paseo del Cauce, 59, Valladolid 47011, Spain.
E-mail address: joseluis.pura@uva.es (J.L. Pura).

https://doi.org/10.1016/j.surfin.2023.102792
Received 4 October 2022; Received in revised form 17 February 2023; Accepted 2 March 2023
Available online 13 March 2023

nanostructured films, the Langmuir-Blodgett (LB) technique stands out for its capacity to obtain highly ordered layers with precise control of the number of deposited layers, while maintaining a relatively simple experimental operation at the same time [19,20]. The LB technique is based on the formation of a molecular monolayer on an aqueous surface, this monolayer is subsequently transferred to a solid substrate. The repetition of the process allows the preparation of multilayers of nanoscale thickness in a controlled manner [21]. This technique offers great advantages such as low price and low density of defects in the monolayers. It also permits great control and consistency of the deposited film thickness and a well-defined and stable molecular arrangement. These capabilities are especially relevant if compared to other conventional deposition techniques, such as spin coating or drop-casting. The LB technique has been adapted for the deposition of different nanomaterials [22]. This has been naturally extended to a broad number of applications including sensing with ZnO NWs [23], surface-enhanced Raman spectroscopy (SERS) on AgNWs [24], or transparent conductive electrodes (TCEs) [25].

Cyclic Voltammetry (CV) is one of the most spread electrochemical techniques, mainly because of the huge amount of information that can be extracted with a simple experimental setup [26,27]. This technique can provide the precise potential at which the redox events occur, but also advanced features like reaction reversibility [28] or electrode reaction kinetics [29] can be extracted from CV measurements. On the other hand, electrochemical impedance spectroscopy (EIS) is a powerful method extensively used for both surface characterization [30–32] and sensing applications [33–35]. EIS is especially appropriate for obtaining valuable information about the condition of the electrode/electrolyte interface and its changes during electrochemical measurements [32]. CV and EIS techniques provide complementary information and are frequently used together to achieve a thorough material characterization [36,37].

Atomic Force Microscopy (AFM) is a remarkable tool to obtain detailed topographic characterizations of nanostructures. Moreover, the coupling of AFM with an electrochemical cell (EC-AFM) makes it possible to monitor and control the evolution of an electrode surface immersed in an electrolytic solution during electrochemical measurements [38]. Two different methodologies can be used for EC-AFM measurements. In the first type, the tip is a passive element (not polarized) that allows scanning of the sample surface and its evolution [39]. Already in 1997, Gewirth et al. studied the effect of cyclic voltammetry on metals and the adsorption of molecules on metal surfaces [40]. The second variant consists of the application of a certain potential to the tip with respect to the surface, allowing the study and detection of local electrochemical reactions on the surface. Alexandrova et al. used a conductive cantilever acting as an electrode to measure proton conductivity through Nafion membranes [41]. Some of the advantages provided by this technique are the high resolution in the x, y, and z directions, and that it does not require extensive sample pretreatment. In addition, images can be directly obtained in an aqueous medium, which allows biological samples to be studied in their native environment, e.g. allowing us to analyze the dynamic transformations of thin films composed of conductive materials and biomolecules without perturbing their bio-functionality [42]. Over the last years, most of the research based on EC-AFM has been focused on the study of surface corrosion [43,44] and Li-ion batteries [45–47], while little attention has been paid to the analysis of sensors' surfaces [48] during operation.

In this work, we present an EC-AFM study of different electrodes modified with AgNWs deposited by the LB technique, which provides homogeneity and reproducibility. The surface condition is monitored by AFM, while the electrodes are electrochemically characterized by CV and EIS. Both boron-doped diamond (BDD) and indium tin oxide (ITO) glass are used as initial electrodes. For both substrates, the studied samples are prepared by two different types of LB deposition: X-type and Z-type. This aims to analyze the role of the electrode/AgNWs LB layer interaction on the electrode performance and aging process.

2. Materials and methods

2.1. Chemicals

Silver nitrate ($AgNO_3$), polyvinylpyrrolidone (PVP, Mw = 55,000), ethylene glycol (EG) anhydrous (99.8%), phosphate buffer, acetone, and ethanol were purchased from Sigma-Aldrich (Saint Louis, MO, USA). Deionized water from MilliQ (Millipore-Sigma Aldrich, Darmstadt, Germany) (resistivity 18.2 MΩcm) was used in all experiments. Potassium chloride (KCl) was provided by PanReac AppliChem (Barcelona, Spain). Boron-doped diamond substrates were provided by NEOCOAT (La Chaux-de-Fonds, Switzerland). Indium tin oxide (ITO) glass substrates were purchased from Sigma-Aldrich (Saint Louis, MO, USA).

2.2. Instruments and methods

The synthesis of the AgNWs was carried out using a Perimax peristaltic pump from Spetec and a Sorvall ST 8 Centrifuge (Thermo Scientific, Walthman, USA), following a modification of the polyol method [14]. The AgNWs are subsequently capped with octanethiol to correctly perform the LB deposition [25].

Micro-Raman spectra were recorded using a high-resolution Labram UV-HR 800 Raman spectrometer from Horiba-JovinYvon. The excitation was carried out with a frequency-doubled Nd:YAG laser (532 nm).

Isotherms measurements and LB film preparation were performed in a KSV-NIMA 5000 (Biolin Scientific) Langmuir-Blodgett trough equipped with a Wilhelmy plate to measure the surface pressure. The octanethiol-capped AgNWs were dissolved in chloroform (20 $mg{\cdot}mL^{-1}$) and mixed in a 10:3 vol ratio with arachidic acid (AA) $4x10^{-4}$ M. The mixture was spread onto ultrapure water (Millipore MilliQ), which was kept at a constant temperature (25 °C).

The surface-area isotherms were registered by compressing the floating molecules at a maximum compression rate of 10 mm/min. At a surface pressure of 45 mN/m, safely apart from collapse, the floating film was transferred to the solid substrate at a maximum speed of 5 mm/min. Monolayers were transferred onto two types of substrates (BDD and ITO).

AFM was used to determine the topography of the films deposited on the BDD and ITO substrates during EC measurements. For this, a Cypher ES Environmental AFM device (Oxford Instruments, Asylum Research, Wiesbaden, Germany) was operated in tapping mode with blueDrive photothermal excitation technology. The tip used was BL-AC40TS (Oxford Instruments, Asylum Research, Wiesbaden, Germany).

Electrochemical measurements, including cyclic voltammetry (CV) and electrochemical impedance spectroscopy (EIS), were carried out using a PGSTAT128 potentiostat/galvanostat (Autolab Metrohm, Utrecht, The Netherlands) in a three-electrode electrochemical cell adapted for EC-AFM measurements. The studied samples are used as the working electrodes, an Ag pseudo-electrode was used as the reference electrode, and a platinum ring (0.6 cm^2) as the counter electrode. The Ag pseudo-electrode was tested versus an $Ag|AgCl/KCl_{sat}$ reference electrode in the same conditions of the electrochemical measurements (i.e. KCl 0.1 M solution) obtaining a stable open circuit potential (OCP) of 0.3975 V.

Scanning electron microscopy (SEM) and Energy Dispersive X-ray Spectroscopy (EDX) measurements were performed in an Environmental SEM, FEI Quanta 200FEG operated at 5 kV for both the acquisition of SEM images and EDX measurements.

3. Results and discussion

Modified electrodes have been prepared by depositing a single layer of AgNWs by LB over BDD and ITO substrates. AgNWs are previously capped with octanethiol to prevent their dissolution in the aqueous phase and make them soluble in chloroform. Prior to the deposition, the isotherms of several LB films are studied. Fig. 1 shows the LB isotherms

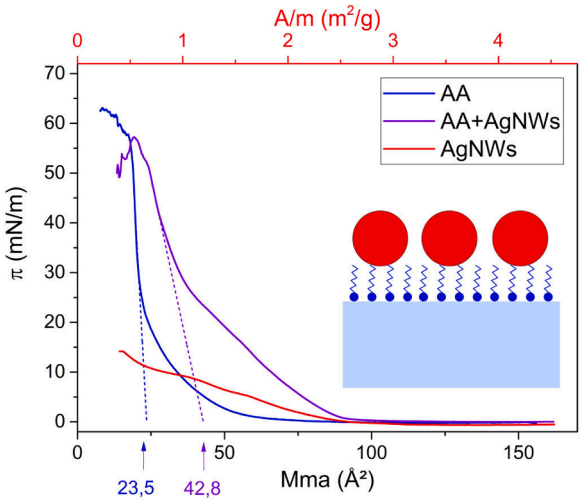

Fig. 1. Langmuir isotherms of arachidic acid (AA), octanethiol-capped AgNWs, and a mixture of both. The inset shows the structure of the Langmuir film.

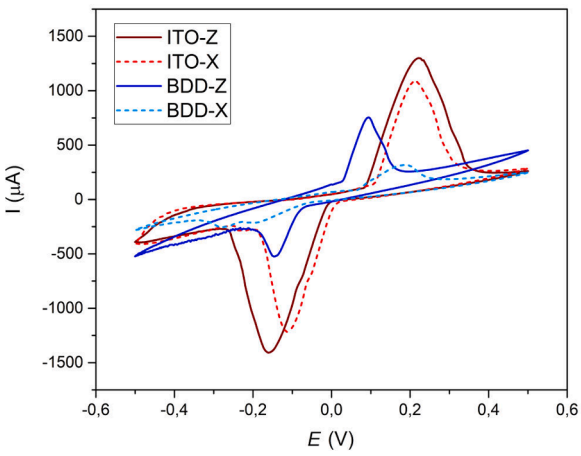

Fig. 2. Cyclic voltammograms of the 4 types of electrodes covered with AA/AgNWs monolayers immersed in 0.1 M KCl. Scan rate 100 mV/s.

of bare arachidic acid (AA), octanethiol-capped AgNWs, and the mixture of both (10:3 vol ratio). AA shows the typical behavior of a classic Langmuir floating monolayer, presenting a collapse surface pressure of 55–6 mN/m. The AgNWs show an almost linear response with no collapse since there are not enough AgNWs for the formation of a dense Langmuir film, only a partial orientation of the AgNWs network is obtained. Finally, when both elements are combined the resulting isotherm is the linear combination of the individual ones. The significant difference in the calculated mean molecular area (Mma) on the solid phase for AA and AA+AgNWs proves the correct inclusion of the AgNWs on the AA film. For the LB film of AgNWs alone, the Mma is replaced by the specific area (A/m) since there is no well-defined value of the AgNWs' molecular weight.

Once the characteristics of the films are known, single monolayers of AA+AgNWs are deposited over BDD and ITO substrates at a surface pressure of 45 mN/m. The deposition is done in both X-type and Z-type LB configurations, this allows for analyzing the effect of the substrate/film interaction on the electrochemical response of the modified electrodes. For the Z-type deposition, the electrodes are submerged before the film preparation and the film is transferred by pulling the electrodes from the liquid phase. For the X-type deposition, the film was prepared and then transferred by introducing the electrodes in the liquid phase. The substrates are prepared in batches of 10 pieces to assess experimental reproducibility and labeled BDD-X, BDD-Z, ITO-X, and ITO-Z, accounting for each substrate and deposition type.

The prepared electrodes underwent EC-AFM measurements on KCl 0.1 M. A single AgNW is selected during AFM inspection, taking an initial topological image of the pristine electrode. After this first assessment, CV measurements are done in situ measuring in the range between −0.5 V and 0.5 V. New AFM images are taken after each cycle with open circuit conditions to keep track of the surface state. The results for all electrodes on the CV cycle number 5 are shown in Fig. 2. This point is selected as the number of CV cycles after which the CV is observed to become stable. In all cases, the observed pair of redox peaks corresponds to the Ag oxidation and reduction of the AgNWs. Both ITO-based electrodes present higher intensity redox peaks than their BDD counterparts, this points to a better electrode/film affinity in the case of ITO. On the other hand, for both ITO and BDD the Z-type electrodes present higher redox intensity, being the difference more noticeable in the case of BDD.

Fig. 3 shows the AFM images of an AA/AgNWs monolayer deposited over ITO. Fig. 3a corresponds to the state before CV, and Figs. 3b–d correspond to the surface state after 1, 2, and 5 cycles, respectively. The AgNWs surface dramatically changes after the EC measurement. Successive CV cycles do not further modify the surface once it is altered, however, the image resolution is progressively lost as a result of undesired AFM tip oxidation, being especially significant in Fig. 3d. It has been confirmed that the surface state remains unchanged after rinsing with deionized water, which rules out the effect of electrode fouling [14, 49], and points to the persistent formation of silver oxide, Ag_2O on the AgNWs surface.

The nature of the AgNWs surface modification has been ascertained by SEM and energy-dispersive X-ray spectroscopy (EDX). Fig. 4 shows an SEM image of one of the samples and the EDX spectra recorded at two points with different surface condition. The presence of Ag is common to both spectra, as well as C (which could come from environmental contamination or octanethiol capping and AA from the LB film). However, the spectrum recorded on top of one of the surface grains shows a significant O peak that is not present in the non-oxidized region. These results confirm that the changes in the AgNW surface condition are linked to the formation of Ag_2O.

The oxidation of the AgNWs surface has been observed as a common factor in all the studied samples. However, there are significant differences in the electrochemical behavior of the four types of studied electrodes as shown in Fig. 2. On the other hand, AFM measurements have proven to be much more difficult for BDD samples as compared to ITO ones. Typically, AgNWs deposited on BDD substrates are removed from the substrate by the cantilever during operation, making the obtention of a stable image truly challenging. In order to fully ascertain the differences between the four types of substrates, a deeper characterization of the samples has been made. First, optical microscopy allowed observing the main structural differences of the deposited monolayers. Second, Micro-Raman spectroscopy permits the verification of the correct deposition of all the elements of the LB film. Finally, a thorough characterization of their electrochemical kinetic response provides information about the underlying charge transfer processes, which has been complemented by an EIS characterization of the samples.

Fig. 5a presents optical images of the studied samples. The morphological differences are obvious. ITO samples present much better ordering in the AgNW structure than BDD samples. On the other hand, Z-Type deposition results in better ordering as compared to X-Type deposition, but also a much better density of AgNWs over the electrode surface, which will directly turn into better performance. Similar results can be observed in Fig. S1, where SEM images are provided. The samples with Z-Type deposition present better ordering of the AgNWs layer.

Fig. 5b shows the micro-Raman spectra of the samples and a bare AgNW for comparison. The two broad peaks in the region 1000–1750 cm^{-1} are common to all samples and also to the bare AgNW and independent of the substrate, so they can be safely attributed to AgNWs. There are 3 especially interesting regions to analyze: 2800–3000 cm^{-1},

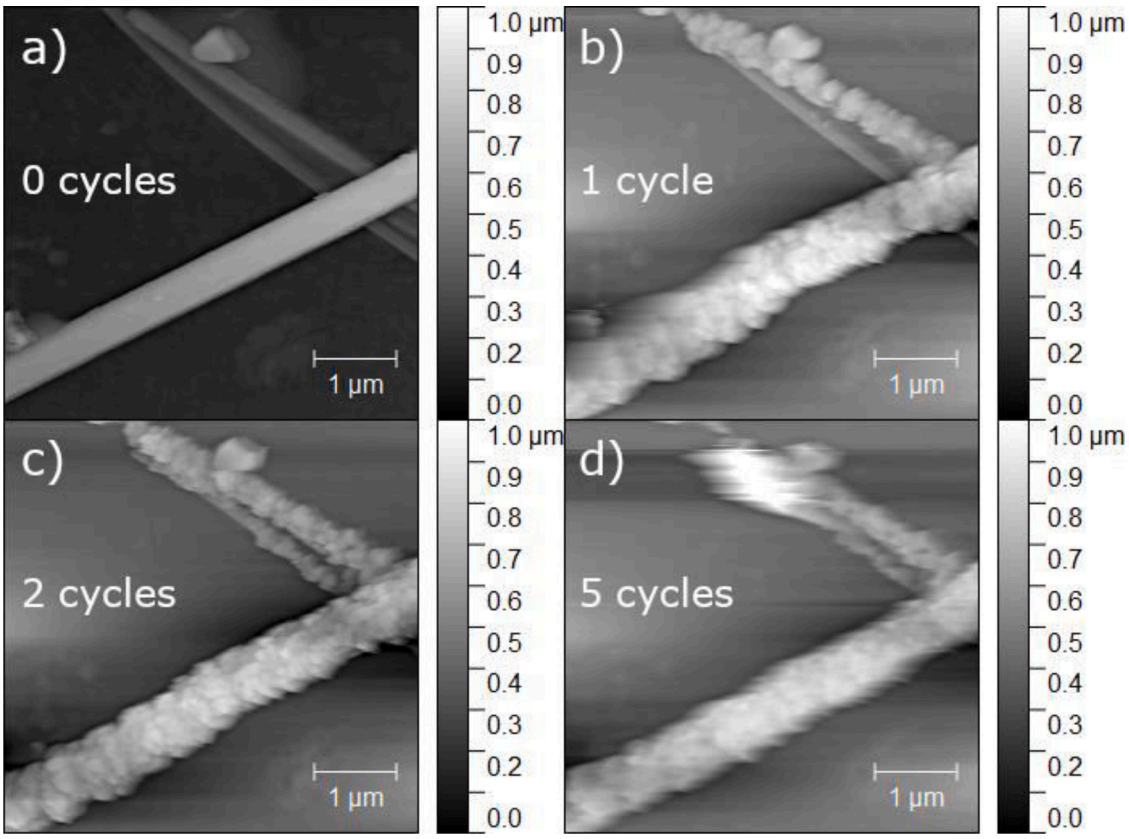

Fig. 3. AFM images of an AA/AgNWs monolayer deposited by LB technique over ITO. The images are obtained in situ after the electrochemical measurements. The images correspond to (a) before CV, (b) after 1 CV cycle, (c) 2 cycles and (d) 5 cycles.

which mainly contains information about the C—H stretch, the region close to 1480 cm^{-1}, associated with the CH_2 bending mode (δ), and the region around 720 cm^{-1}, corresponding to the CH_2 rocking-twisting [50,51]. All of these vibrational modes are characteristic of alkanes, which confirms the deposition of the capped AgNWs together with the AA film. It is also worth noting that in both Z-type electrodes, these three signals are much better observed than for X-type electrodes, which is especially clear in the CH peaks (2800–3000 cm^{-1} region). This manifests again the key importance of the film/substrate interaction, which seems much better for Z-type deposition regardless of the substrate used and is in perfect agreement with the rest of the experiments.

The results of the kinetic response of the studied electrodes are summarized in Fig. 6. All the samples have been measured for increasing values of the scan rate: 10, 20, 50, 100, 200, 500, and 1000 mV/s. All of them show similar trends: higher peak intensity and higher full-width half maximum (FWHM) when increasing the scan rate, as expected. The dependence of the oxidation peak potential on the scan rate can be studied by means of the Laviron equation [52]:

$$E_a = E^0 + \frac{RT}{(1-\alpha)nF}\log\left[\frac{(1-\alpha)nF}{RT}\frac{\nu}{k_s}\right] \quad (1)$$

where E_a is the peak potential of the anodic peak, E^0 is the reference oxidation potential, α is the charge transfer coefficient, n is the number of electrons of the oxidation process, k_s is the rate constant of the electrochemical reaction, and ν is the scan rate. The fitting of Eq. (1) to the experimental data in Fig. 6 allows us to calculate the value of the charge transfer coefficient α, which in this case ($n = 1$) is equivalent to the symmetry coefficient. The results are summarized in Table 1. The values of α for ITO are really close to 0.5, while for BDD are significantly far from 0.5, even exceeding unity for BDD-X samples.

In a parallel way it is possible to calculate the value of α according to the Butler-Volmer equation, which can be simplified for large values of the overpotential (η > 118 mV) [53,54]:

$$\ln I = \ln I_0 - \frac{(1-\alpha)F}{RT}\eta \quad (2)$$

By plotting (ln I) vs η, which is known as a Tafel plot, we can obtain the slope of the fit and therefore the value of α according to Eq. (2). Fig. S2 shows the Tafel plots for all samples, and the calculated values of α have been added to Table 1 for comparison. The trend is identical to the Laviron results supporting previous results. It is important to note that typically the results obtained from the Laviron equation are more robust than those obtained by fitting the Tafel plot.

Another interesting parameter that can be obtained from the kinetic CV is the surface concentration of the mediator, Γ_O. It can be obtained from the area of the anodic peak at the lowest value of the scan rate (10 mV/s). The intensity in CV depends on Γ_O according to the following equation [52]:

$$i_a = -nFA\frac{d\Gamma_O}{dt} = -nFA\frac{d\Gamma_O}{dE}\frac{dE}{dt} = -nFA\nu\frac{d\Gamma_O}{dE} \quad (3)$$

Where A is the area of the electrode, $dE/dt = \nu$, is the scan rate. Then, we can integrate both sides and the left-hand side will be the integral of i_a over the potential E, i.e. the area of the anodic peak, I. By simplifying we can obtain Γ_O:

$$\Gamma_O = \frac{I}{nFA} \quad (4)$$

The values of Γ_O are summarized in Table 1. The calculated surface concentration of the mediator is higher for ITO substrates than for BDD ones, and also higher values are obtained for Z-type deposition as compared to X-type.

All of these results are in good agreement with the better electrochemical response observed for AgNWs deposited onto ITO as compared

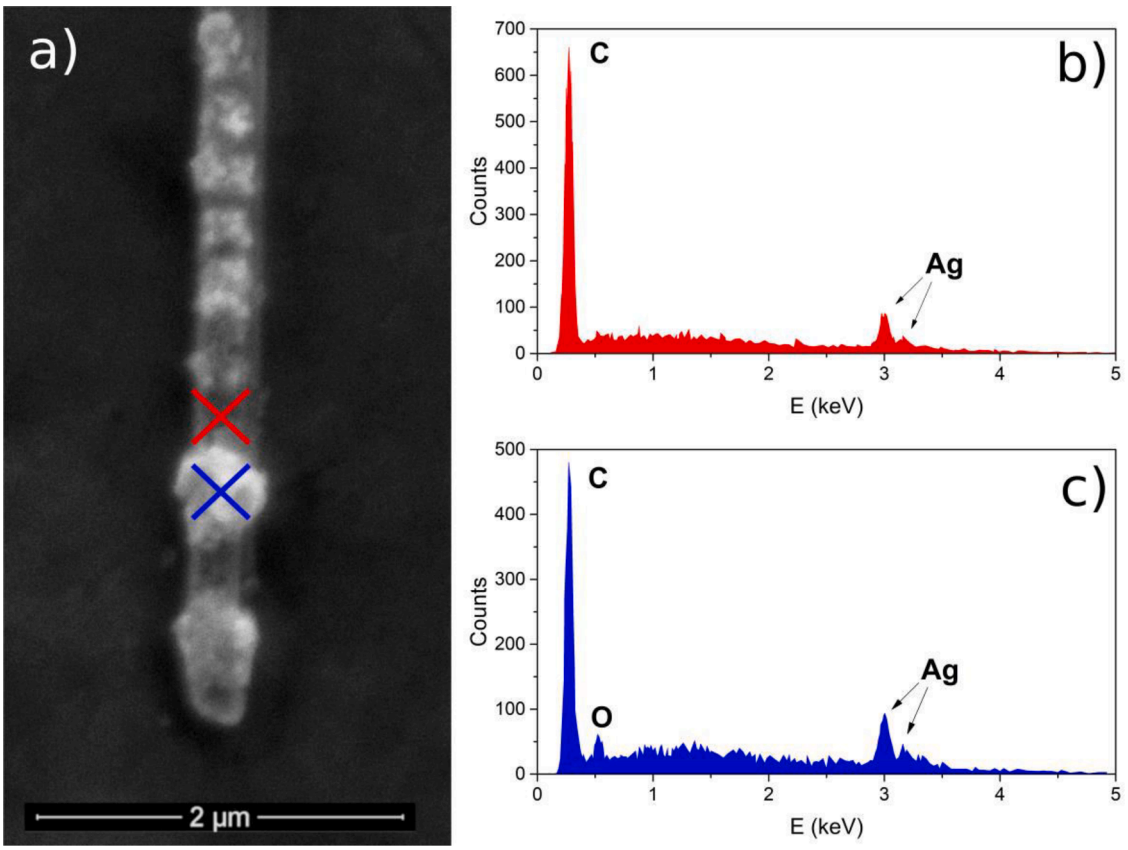

Fig. 4. (a) SEM image of an AgNW after 5 CV cycles with a potential of 5 kV. (b) and (c) EDX spectra were recorded in two different regions of the AgNW surface: on the clear AgNW surface region (red), and over one of the bright contrast grains (blue). The signal of Ag can be observed in both cases, as well as C contamination. However, a significant O signal is only present on the spectra recorded in the grain.

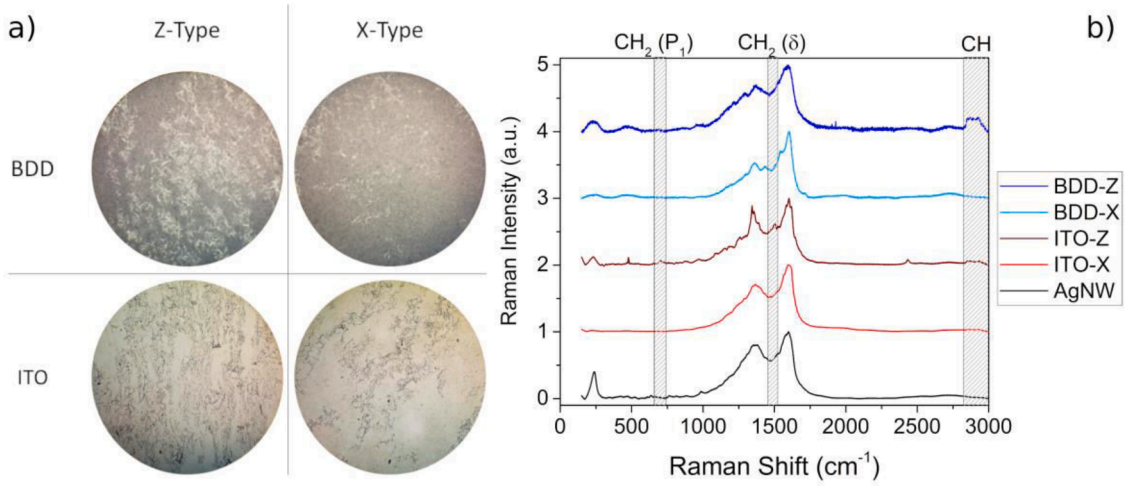

Fig. 5. (a) Optical images (10X magnification) of the four types of samples. (b) Micro-Raman spectra of the samples and bare AgNWs for comparison.

to BDD and manifest the importance of the modifier/substrate interaction and its link with the electrochemical reversibility. When the AgNWs/substrate interface is not optimal the intrinsic response of the electrode departs from the ideal regime. This effect becomes especially noticeable after the data analysis, i.e. the calculated values of α; however, it can be directly observed in Fig. 6 where the intensity of BDD samples is lower and presents more noise, being again more clear for BDD-X samples.

To finish the characterization of the samples, we performed EIS measurements. The results are summarized in Figs. 7 and 8. Fig. 7 shows a Bode plot of the evolution of the ITO-Z sample with the number of CV cycles, the response is analogous for the 4 different groups of samples. The most dramatic change takes place on the first CV cycle, corresponding to the AgNWs surface oxidation. After the first cycle, the changes are significantly more subtle, reaching equilibrium after 4–5 cycles, the same behavior observed in the CV measurements. Fig. 8 shows a comparison of the 4 electrodes for the two limiting cases: previous to any CV cycle and after reaching equilibrium, 5 CV cycles. Two different tendencies are clear: one for ITO electrodes and the other for BDD electrodes. BDD always shows lower values of the impedance

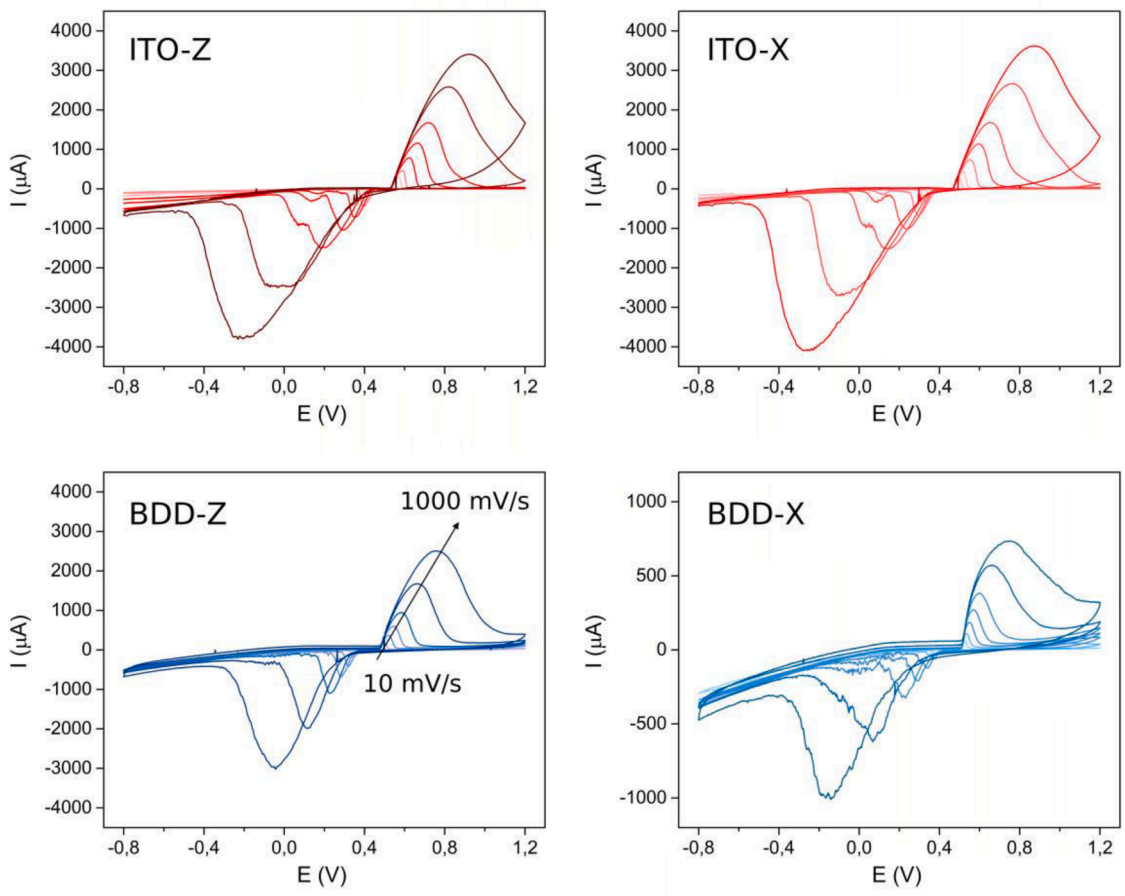

Fig. 6. CV measurements of the 4 groups of modified electrodes for increasing values of the scan rate: 10, 20, 50, 100, 200, 500, and 1000 mV/s. In all of them, the Ag redox peaks show similar trends: higher intensity and higher peak FWHM when increasing the scan rate.

Table 1
Calculated values of the charge transfer coefficient α using both the Laviron equation and Tafel plots, the surface concentration of the modifier Γ_O and the capacitance of the samples before CV, C_0, and after 5 CV cycles, C_5.

	α (Laviron)	α (Tafel)	Γ_O /mol·cm^{-2}	C_0/μF	C_5/μF
ITO-Z	0.5011	0.4527	$2.21 \cdot 10^{-8}$	3.034	14.704
ITO-X	0.4882	0.3763	$1.85 \cdot 10^{-8}$	2.803	12.858
BDD-Z	0.1739	0.2295	$6.18 \cdot 10^{-9}$	42.864	80.381
BDD-X	−0.0980	0.2283	$5.17 \cdot 10^{-9}$	25.283	49.001

modulus, especially noticeable at high frequencies, which agrees with its intrinsically higher electrical conductivity. On the other hand, lower values of the impedance modulus can be observed for Z-type electrodes as compared to X-type electrodes, pointing to a better AgNWs/electrode interaction and supporting all previous results. The capacitance of the system can be determined from the impedance values, the calculated values are gathered in Table 1. According to previous results, the capacitance increases after 5 CV cycles with a 5-fold increase for ITO samples and a 3-fold increase for BDD. This is in perfect agreement with the formation of a dielectric Ag_2O shell on the AgNWs surface observed on AFM and SEM images. Finally, the phase plot also shows a significant shift of the curves to lower frequencies after the 5 CV cycles, which confirms the capacitance growth.

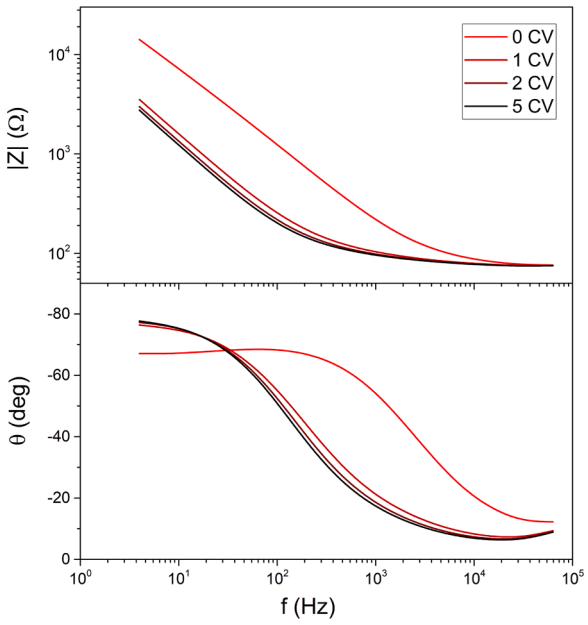

Fig. 7. Bode plot of the EIS measurements of AgNWs modified ITO-Z electrode for a different number of CV cycles. The most dramatic change takes place on the first CV cycle matching the AgNWs surface oxidation. After the first cycle, the changes are significantly more subtle, reaching equilibrium after 4–5 cycles, as observed in CV.

4. Conclusions

The silver nanowires (AgNWs) modified electrodes prepared by the Langmuir-Blodgett (LB) technique have been in-situ characterized during electrochemical atomic force microscopy (EC-AFM) measurements.

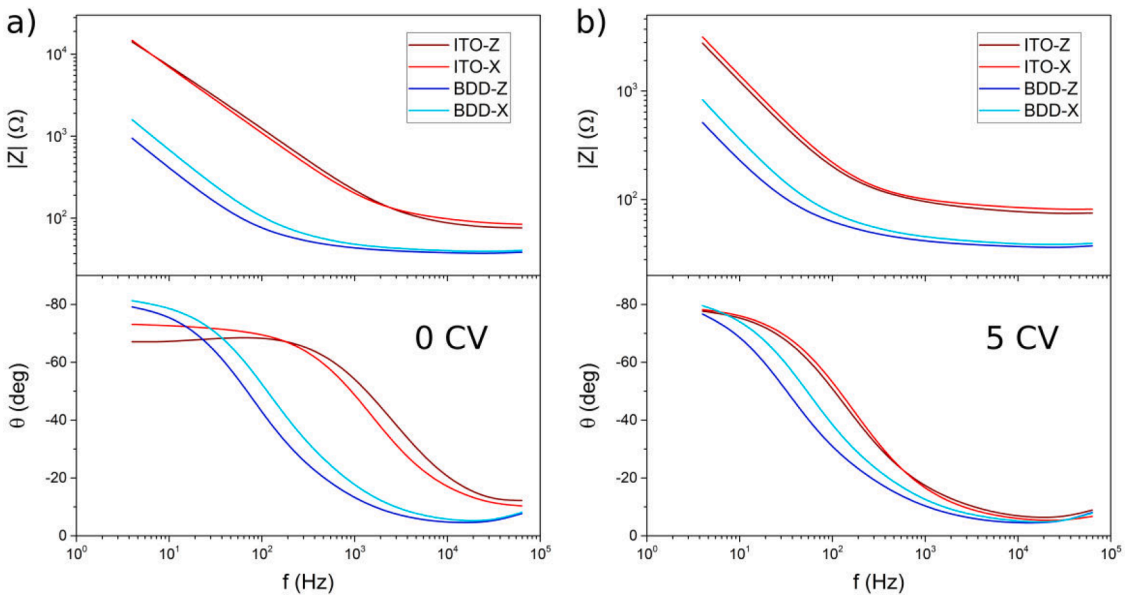

Fig. 8. Bode plot of the 4 electrodes for comparison: (a) previous to any CV cycle, (b) After 5 CV cycles. The capacitance of the system, given by the slope of the linear part of the impedance modulus plot, increases after the CV, in good agreement with the formation of Ag_2O on the AgNWs surface.

This approach allowed for a detailed study of the electrode surface condition and its modification during EC activity. AFM images exhibit the formation of Ag_2O over the NW surface as a result of cyclic voltammetry (CV), which has been confirmed by scanning electron microscopy and energy-dispersive X-ray spectroscopy. Furthermore, electrochemical impedance spectroscopy showed the direct effect of the Ag_2O layer on the modification of the electrode capacitance. The kinetic EC response of the modified electrodes complemented the CV measurements, unveiling critical differences in the 4 types of LB deposition. Indium tin oxide (ITO)-based electrodes present better EC characteristics than boron-doped diamond (BDD)-based electrodes, despite the higher electrical conductivity of BDD.

The results demonstrate that Z-type deposition achieves better electrode performance for both ITO and BDD in comparison with X-type, independently of the hydrophobic/hydrophilic nature of the substrates. This proves that the interaction between the electrode and the possible modifiers is of key importance for the performance of the modified electrode, with a significant impact on the charge transfer processes.

The simultaneous analysis of the EC and AFM of modified electrodes opens the door to analyzing the subtle relationship between the modifying materials and the electrode substrate, which will directly impact the performance of the electrodes in the desired applications. This work also supports the viability of the EC-AFM technique to approach open problems involving electrochemistry and surface science.

CRediT authorship contribution statement

Jose Luis Pura: Conceptualization, Investigation, Methodology, Formal analysis, Writing – original draft, Writing – review & editing. **Coral Salvo-Comino:** Investigation, Methodology. **Cristina García-Cabezón:** Methodology, Formal analysis, Supervision. **María Luz Rodríguez-Méndez:** Conceptualization, Funding acquisition, Methodology, Supervision, Writing – review & editing.

Declaration of Competing Interest

The authors declare that they have no known competing financial interests or personal relationships that could have appeared to influence the work reported in this paper.

Data availability

Data will be made available on request.

Acknowledgments

The authors appreciate the financial support of MINECO-FEDER Plan Nacional (RTI2018–097990-B-100), Junta de Castilla y Leon-FEDER VA202P20 and «Infraestructuras Red de Castilla y León (INFRARED)» UVA01, the EU-FEDER program (CLU-2019–04), and the European Union–NextGenerationEU and the University of Valladolid (CONVREC-2021–23).

Supplementary materials

Supplementary material associated with this article can be found, in the online version, at doi:10.1016/j.surfin.2023.102792.

References

[1] F. Terzi, L. Pigani, C. Zanardi, Unusual metals as electrode materials for electrochemical sensors, Curr. Opin. Electrochem. 16 (2019) 157–163.
[2] J. Barek, J. Fischer, T. Navrátil, K. Pecková, B. Yosypchuk, J. Zima, Nontraditional electrode materials in environmental analysis of biologically active organic compounds, Electroanalysis 19 (2007) 19–20, 2003–2014.
[3] R.L. McCreery, Advanced carbon electrode materials for molecular electrochemistry, Chem. Rev. 108 (7) (2008) 2646–2687.
[4] T.Y. Huang, J.H. Huang, H.Y. Wei, K.C. Ho, C.W. Chu, RGO/SWCNT composites as novel electrode materials for electrochemical biosensing, Biosens. Bioelectron. 43 (1) (2013) 173–179.
[5] H. Luo, Z. Shi, N. Li, Z. Gu, Q. Zhuang, Investigation of the electrochemical and electrocatalytic behavior of single-wall carbon nanotube film on a glassy carbon electrode, Anal. Chem. 73 (5) (2001) 915–920.
[6] L. Chen, Y. Tang, K. Wang, C. Liu, S. Luo, Direct electrodeposition of reduced graphene oxide on glassy carbon electrode and its electrochemical application, Electrochem. commun. 13 (2) (2011) 133–137.
[7] L. Zhang, X. Jiang, E. Wang, S. Dong, Attachment of gold nanoparticles to glassy carbon electrode and its application for the direct electrochemistry and electrocatalytic behavior of hemoglobin, Biosens. Bioelectron. 21 (2) (2005) 337–345.
[8] K. Brainina, N. Stozhko, M. Bukharinova, E. Vikulova, Nanomaterials: electrochemical Properties and Application in Sensors, Phys. Sci. Rev. 3 (9) (2019) 20188050.
[9] D.R. Bagal-Kestwal, M.H. Pan, B.H. Chiang, Electrically nanowired-enzymes for probe modification and sensor fabrication, Biosens. Bioelectron. 121 (June) (2018) 223–235.

[10] C. Salvo-Comino, A. González-Gil, J. Rodriguez-Valentin, C. Garcia-Hernandez, F. Martin-Pedrosa, C. Garcia-Cabezon, M.L. Rodriguez-Mendez, Biosensors platform based on chitosan/AuNPs/phthalocyanine composite films for the electrochemical detection of catechol. the role of the surface structure, Sensors 20 (7) (2020) 1–12. Switzerland.

[11] C. Zhang, S. Govindaraju, K. Giribabu, Y.S. Huh, K. Yun, AgNWs-PANI nanocomposite based electrochemical sensor for detection of 4-nitrophenol, Sens. Actuators B Chem. 252 (2017) 616–623.

[12] L. Xu, Y. Hou, M. Zhang, T. Cheng, W. Huang, C. Yao, Q. Wu, Electrochemical sensor based on silver nanowires modified electrode for determination of cholesterol, Anal. Methods 7 (2015) 5649–5653.

[13] U. Yogeswaran, S.M. Chen, A review on the electrochemical sensors and biosensors composed of nanogaps as sensing material, Sensors 8 (2008) 290–313. Switzerland.

[14] C. Salvo-Comino, F. Martin-Pedrosa, C. Garcia-Cabezon, M.L. Rodriguez-Mendez, Silver nanowires as electron transfer mediators in electrochemical catechol biosensors, Sensors 21 (3) (2021) 1–13. Switzerland.

[15] H.G. Im, J. Jang, Y. Jeon, J. Noh, J. Jin, J.Y. Lee, B.S. Bae, Flexible transparent crystalline-ITO/Ag nanowire hybrid electrode with high stability for organic optoelectronics, ACS Appl. Mater. Interfaces 12 (50) (2020) 56462–56469.

[16] Y. Yi, G. Weinberg, M. Prenzel, M. Greiner, S. Heumann, S. Becker, R. Schlögl, Electrochemical corrosion of a glassy carbon electrode, Catal. Today 295 (July) (2017) 32–40.

[17] A.M. Fenelon, C.B. Breslin, The electrochemical synthesis of polypyrrole at a copper electrode: corrosion protection properties, Electrochim. Acta 47 (28) (2002) 4467–4476.

[18] M.X. Qiao, Y. Zhang, L.F. Zhai, M. Sun, Corrosion of graphite electrode in electrochemical advanced oxidation processes: degradation protocol and environmental implication, Chem. Eng. J. 344 (January) (2018) 410–418.

[19] R.H. Tredgold, The physics of langmuir-Blodgett films, Rep. Prog. Phys. 50 (12) (1987) 1609–1656.

[20] K. Ariga, Y. Yamauchi, T. Mori, J.P. Hill, 25th Anniversary article: what can be done with the langmuir-blodgett method? Recent developments and its critical role in materials science, Adv. Mater. 25 (45) (2013) 6477–6512.

[21] I.R. Peterson, langmuir-Blodgett films, J. Phys. D. Appl. Phys. 23 (1990) 379–395.

[22] S. Acharya, J.P. Hill, K. Ariga, Soft langmuir-blodgett technique for hard nanomaterials, Adv. Mater. 21 (29) (2009) 2959–2981.

[23] C. Baratto, V. Golovanova, G. Faglia, H. Hakola, T. Niemi, N. Tkachenko, B. Nazarchurk, V. Golovanov, On the alignment of ZnO nanowires by Langmuir – Blodgett technique for sensing application, Appl. Surf. Sci. 528 (May) (2020), 146959.

[24] A. Tao, F. Kim, C. Hess, J. Goldberger, R. He, Y. Sun, Y. Xia, P. Yang, Langmuir-Blodgett silver nanowire monolayers for molecular sensing using surface-enhanced Raman spectroscopy, Nano Lett. 3 (9) (2003) 1229–1233.

[25] D. Lopez-Diaz, C. Merino, M.M. Velázquez, Modulating the optoelectronic properties of silver nanowires films: effect of capping agent and deposition technique, Materials 8 (11) (2015) 7622–7633. Basel.

[26] D.H. Evans, K.M. O'Connell, R.A. Petersen, M.J. Kelly, Cyclic voltammetry, J. Chem. Educ. 60 (4) (1983), 290.

[27] J.F. Rusling, S.L. Suib, Characterizing materials with cyclic voltammetry, Adv. Mater. 6 (12) (1994) 922–930.

[28] R.J. Klingler, J.K. Kochi, Electron-transfer kinetics from cyclic voltammetry. Quantitative description of electrochemical reversibility, J. Phys. Chem. 85 (12) (1981) 1731–1741.

[29] R.S. Nicholson, Theory and application of cyclic voltammetry for measurement of electrode reaction kinetics, Anal. Chem. 37 (11) (1965) 1351–1355.

[30] B.Y. Chang, S.M. Park, Electrochemical impedance spectroscopy, Annu. Rev. Anal. Chem. 3 (1) (2010) 207–229.

[31] K. Jüttner, Electrochemical impedance spectroscopy (EIS) of corrosion processes on inhomogeneous surfaces, Electrochim. Acta 35 (10) (1990) 1501–1508.

[32] J. Muñoz, R. Montes, M. Baeza, Trends in electrochemical impedance spectroscopy involving nanocomposite transducers: characterization, architecture surface and bio-sensing, Trends Anal. Chem. 97 (2017) 201–215.

[33] I.I. Suni, Impedance methods for electrochemical sensors using nanomaterials, TrAC - Trends Anal. Chem. 27 (7) (2008) 604–611.

[34] F. Lisdat, D. Schäfer, The use of electrochemical impedance spectroscopy for biosensing, Anal. Bioanal. Chem. 391 (5) (2008) 1555–1567.

[35] C. Brett, Electrochemical impedance spectroscopy for characterization of electrochemical sensors and biosensors, ECS Meet. Abstr. 26 (2008) 904. MA2008-01–904.

[36] O. Gharbi, M.T.T. Tran, B. Tribollet, M. Turmine, V. Vivier, Revisiting cyclic voltammetry and electrochemical impedance spectroscopy analysis for capacitance measurements, Electrochim. Acta (343) (2020), 136109.

[37] L. Han, H. Ju, Y. Xu, Ethanol electro-oxidation: cyclic voltammetry, electrochemical impedance spectroscopy and galvanostatic oscillation, Int. J. Hydrog. Energy 37 (20) (2012) 15156–15163.

[38] J.P. Bearinger, C.A. Orme, J.L. Gilbert, Direct observation of hydration of TiO_2 on Ti using electrochemical AFM: freely corroding versus potentiostatically held, Surf. Sci. 491 (3) (2001) 370–387.

[39] J.V. Macpherson, P.R. Unwin, Noncontact electrochemical imaging with combined scanning electrochemical atomic force microscopy, Anal. Chem. 73 (3) (2001) 550–557.

[40] A.A. Gewirth, B.K. Niece, Electrochemical applications of in situ scanning probe microscopy, Chem. Rev. 97 (4) (1997) 1129–1162.

[41] E. Aleksandrova, R. Hiesgen, D. Eberhard, K.A. Friedrich, T. Kaz, E. Roduner, Proton conductivity study of a fuel cell membrane with nanoscale resolution, ChemPhysChem 8 (4) (2007) 519–522.

[42] J.S. Jeong, G. Dietler, Controlling a single DNA molecule in an electric field by means of *in situ* atomic force microscopy, J. Electrochem. Soc. 159 (7) (2012) H623–H625.

[43] P. Yi, C. Dong, K. Xiao, X. Li, Study on corrosion behavior of β-Sn and intermetallic compounds phases in SAC305 alloy by in-situ EC-AFM and first-principles calculation, Corros. Sci. 181 (January) (2021), 109244.

[44] H. Chen, Z. Qin, M. He, Y. Liu, Z. Wu, Materials 13 (3) (2020) 668.

[45] R. Vidu, F.T. Quinlan, P. Stroeve, Use of *in situ* electrochemical atomic force microscopy (EC-AFM) to monitor cathode surface reaction in organic electrolyte, Ind. Eng. Chem. Res. 41 (25) (2002) 6546–6554.

[46] C. Shen, G. Hu, L.Z. Cheong, S. Huang, J.G. Zhang, D. Wang, Direct observation of the growth of lithium dendrites on graphite anodes by operando EC-AFM, Small Methods 2 (2018), 1700298.

[47] H. Zhang, D. Wang, C. Shen, *In-situ* EC-AFM and *ex-situ* XPS characterization to investigate the mechanism of SEI formation in highly concentrated aqueous electrolyte for Li-ion batteries, Appl. Surf. Sci. 507 (September 2019) (2020), 145059.

[48] M.R. Nellist, F.A.L. Laskowski, J. Qiu, H. Hajibabaei, K. Sivula, T.W. Hamann, S. W. Boettcher, Potential-sensing electrochemical atomic force microscopy for in operando analysis of water-splitting catalysts and interfaces, Nat. Energy 3 (1) (2018) 46–52.

[49] B.L. Hanssen, S. Siraj, D.K.Y. Wong, Recent strategies to minimise fouling in electrochemical detection systems, Rev. Anal. Chem. 35 (1) (2016) 1–28.

[50] F. Bensebaa, T.H. Ellis, E. Kruus, R. Voicu, Y. Zhou, Characterization of self-assembled bilayers: silver−Alkanethiolates, Langmuir 14 (22) (1998) 6579–6587.

[51] R.G. Snyder, J.H. Schachtschneider, Vibrational analysis of the n-paraffins—I, Spectrochim. Acta 19 (1) (1963) 85–116.

[52] E. Laviron, General expression of the linear potential sweep voltammogram in the case of diffusionless electrochemical systems, J. Electroanal. Chem. 101 (1) (1979) 19–28.

[53] C. Salvo-Comino, C. Garcia-Hernandez, C. Garcia-Cabezon, M.L. Rodriguez-Mendez, Promoting laccase sensing activity for catechol detection using LBL assemblies of chitosan/ionic liquid/phthalocyanine as immobilization surfaces, Bioelectrochemistry 132 (2020), 107407.

[54] G. Inzelt, Milestones of the development of kinetics of electrode reactions, J. Solid State Electrochem. 15 (7–8) (2011) 1373–1389.